
Article:
Zhang, K., Li, G.-J. orcid.org/0000-0002-5956-4033, Zhu, Z.Q. et al. (1 more author) (2020) Analytical modelling of dynamic performance with harmonic current injection for doubly salient SynRMs. IEEE Transactions on Industry Applications, 56 (4). pp. 3477-3487. ISSN 0093-9994

https://doi.org/10.1109/TIA.2020.2982858

Analytical Modelling of Dynamic Performance with Harmonic Current Injection for Doubly Salient SynRMs

K. Zhang, G. J. Li, *Senior Member*, *IEEE*, Z. Q. Zhu, *Fellow*, *IEEE*, and G. W. Jewell
Department of Electronic and Electrical Engineering, The University of Sheffield, Sheffield, UK
g.li@sheffield.ac.uk

***Abstract*—A new analytical torque model based on *dq0*-axis frame has been developed for 3-phase, 12-slot/8-pole single layer doubly salient synchronous reluctance machines. This newly developed torque model, compared to the one often based on *abc*-axis frame, is necessary to simplify the investigation of dynamic performance such as torque-speed curve and efficiency maps. It has been found that the 3rd order current harmonic injection not only improves the torque performance (increased average torque and reduced torque ripple) in constant torque region, but also maintains a similar torque level as the fundamental current supply in the flux weakening region. Moreover, although the 5th and 7th order current harmonic injection can reduce the torque ripple of machine, their dynamic performances are compromised due to low average torque and significant voltage distortion. Finite element simulations and dynamic tests have been carried out to prove the accuracy of the developed torque model and also the efficiency of the proposed current harmonic injection method.**

***Keywords*—doubly salient, harmonic current injection, synchronous reluctance machine, torque ripple reduction.**

I. INTRODUCTION

Recently, switched reluctance machines (SRMs) have attracted increasing interest for high-performance applications due to their robustness, simplicity and low manufacturing cost [1]. Without any permanent magnets or field windings on the rotor, SRMs are excellent for harsh environment and safety-critical applications [2]. However, despite the SRMs having these and other attractive features, an asymmetric converter is often needed due to the specific current supply mode, as a result the use of conventional SRMs (CSRMs) in a wider range of industrial applications has been restricted. In addition, the doubly salient structure is regarded as one of the main factors that contributes to their high torque ripple, high vibrations and acoustic noise compared to the permanent magnet machines or induction machines.

In most of the available literature about SRMs, many researchers have focused on investigating innovative methods to reduce the vibrations and acoustic noise. Apart from the well-established fact that the radial force excitation is the primary source of vibrations and acoustic noise [3], the torque ripple of SRMs has also been identified as another source determined by the tangential magnetic force [4]. In order to reduce the vibrations and acoustic noise, many studies have been carried out from the design or control aspects of the SRMs. In [5], authors mounted two or more SRMs in parallel sharing the same rotor shaft in order to reduce torque ripple and acoustic noise. In [6], rotor and/or stator shaping and skewing were investigated to minimize the torque ripple. Apart from the aforementioned design techniques, control strategies such as adopting different current excitations can also significantly reduce torque ripple and vibrations. For the square wave current supply, authors in [7] have proposed a torque sharing function to smooth the torque production during phase commutation. In [8], the direct instantaneous torque control (DITC) was proposed to reduce the torque ripple. Sinusoidal excitation effects on radial force have also been investigated for SRMs [9]. Moreover, other current waveform shaping methods have been considered to reduce torque ripple and vibrations and acoustic noise [10].

In addition to the above methods, authors in [11] proposed a mutually coupled SRM (MCSRM), as shown in Fig. 1, that can also achieve lower vibrations and acoustic noise compared to the CSRMs, especially when the sinewave current supply is adopted. It is worth mentioning that with sinewave current supply, the MCSRM becomes essential a doubly salient synchronous reluctance machine (SynRM). It is also found that, at relatively high phase current levels, the MCSRM can produce an average torque twice as high as that of the CSRM. However, MCSRMs also produces much higher torque ripple, leading to potentially higher vibrations and acoustic noise.

In order to reduce the torque ripple of MCSRM, a new method of current harmonic injection is proposed in [12]-[13]. In these papers, the idea is to inject a single current harmonic with predicted magnitude and phase angle to obtain an opposite torque ripple component (torque due to harmonic current) to that produced by fundamental current (torque due to fundamental current). As a result, the resultant torque ripple can be significantly reduced. A torque model using electromagnetic quantities in *abc*-axis frame such as 3-phase self- and mutual-inductances, 3-phase currents, etc. has been developed in [12]-[13], which allows to predict the current harmonics (order, amplitude and phase angle) that need to be injected to reduce the torque ripple and/or to increase the average torque. However, the injected harmonic currents together with inductance harmonics would lead to non-negligible voltage distortion, which might influence machines' dynamic performance such as torque-speed curves and efficiency maps. This has not been studied before and will be the main focus of this paper.

The models developed in [12]-[13] using electromagnetic quantities in *abc*-axis frame are quite complex for analysis due to large number of parameters that need to be considered, e.g. 3-phase currents (fundamental and also harmonic components), 3-phase self- and mutual-inductances, etc. This is particularly the case for analyzing dynamic performance such as torque-speed and power-speed curves, efficiency maps, etc. To simplify the modelling for dynamic performance analyses, a common approach adopted in literature such as in [14]-[16] is to decouple the electromagnetic quantities from stationary (*abc*-axis) reference frame into rotating (*dq*-axis) reference frame.

However, in such electromagnetic models of synchronous reluctance machines, only the dc and 2nd order harmonics of the self- and mutual-inductances are considered. As a result, the *dq*-axis equivalents, such as, the *dq*-axis flux linkages and electromagnetic torque become constant (no torque ripple is considered). This means that the influence of higher order inductance harmonics cannot be fully considered. Although some existing research papers consider the higher order harmonic inductances in the electromagnetic model of synchronous reluctance machines [17]-[18], they often neglect the influence of current harmonics on machine performances. Therefore, in order to provide a more complete insight into the mechanism of torque generation and particularly to simplify the dynamic performance analyses of the MCSRMs with harmonic current injections, an alternative torque model based on *dq0*-axis frame that consider both current and inductance harmonics will be proposed in this paper.

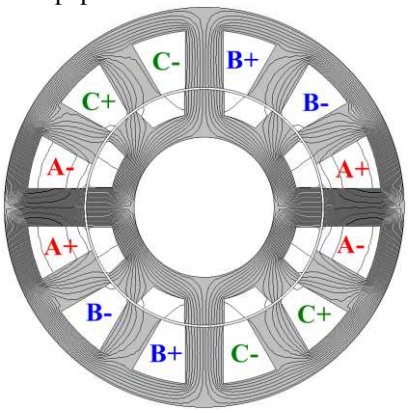

Fig. 1. Cross section and winding configuration of a 12s/8p single layer MCSRM. Here only the phase A is supplied with a dc current.

TABLE I MACHINE KEY DIMENSIONS AND DESIGN FEATURES

Stator slot number	12	Rotor inner radius (mm)	15.7
Rotor pole number	8	Active length (mm)	60
Stator outer radius (mm)	45	Number of turns per phase	132
Air gap length (mm)	0.5	Coil packing factor	0.37
Rotor outer radius (mm)	26.5	Current density (A_{rms}/mm^2)	5.68

II. INSTANTANEOUS TOQUE EQUATION WITH FUNDAMENTAL CURRENT SUPPLY

It is well-established that a balanced 3-phase voltages of a synchronous reluctance machine is given by (1), which can also be employed for a MCSRM [18].

$$[v]_{abc} = R[i]_{abc} + \frac{d[\psi]_{abc}}{dt} \tag{1}$$

$$[\psi]_{abc} = [L_s][i]_{abc} \tag{2}$$

where $[v]_{abc}$, $[i]_{abc}$ and $[\psi]_{abc}$ are stator voltages, currents and flux linkages, respectively. R and $[L_s]$ represent the stator resistance and 3-phase inductance matrix, respectively.

$$L_s = \begin{bmatrix} L_{aa} & M_{ab} & M_{ac} \\ M_{ba} & L_{bb} & M_{bc} \\ M_{ca} & M_{cb} & L_{cc} \end{bmatrix} \tag{3}$$

where L and M are the self- and mutual-inductances and given by:

$$\begin{cases} L_{xx}(\theta_e) = L_{s0} + \sum_{n=2,4,6,\dots}^{\infty} L_n \cos(n(\theta_e + \theta_{xx})) \\ M_{xy}(\theta_e) = M_{s0} + \sum_{n=2,4,6,\dots}^{\infty} M_n \cos(n(\theta_e + \theta_{xy})) \end{cases} \tag{4}$$

where x and y indicate the phases a, b and c. L_{s0} and L_n are the dc component and the magnitude of the n^{th} order self-inductance harmonic, while M_{s0} and M_2 are the dc component and the magnitude of the nth order mutual-inductance harmonic. θ_{xx} is the phase shift angle between three phases. For the investigated machine, it is equal to $0°$, $-120°$ and $120°$, for phases a, b and c, respectively. However, θ_{xy} is equal to $120°$, $0°$ and $-120°$, between phases a and b, b and c and c and a, respectively. After implementing the Park transformation P for (1)-(4), the standard *dq0*-axis model can be derived as

$$P = \begin{bmatrix} \cos\theta_e & -\sin\theta_e & 1 \\ \cos(\theta_e - 120°) & -\sin(\theta_e - 120°) & 1 \\ \cos(\theta_e + 120°) & -\sin(\theta_e + 120°) & 1 \end{bmatrix} \tag{5}$$

$$\begin{bmatrix} v_d \\ v_q \\ v_0 \end{bmatrix} = R\begin{bmatrix} i_d \\ i_q \\ i_0 \end{bmatrix} + \begin{bmatrix} 0 & -\omega & 0 \\ \omega & 0 & 0 \\ 0 & 0 & 0 \end{bmatrix}\begin{bmatrix} \psi_d \\ \psi_q \\ \psi_0 \end{bmatrix} + \frac{d}{dt}\begin{bmatrix} \psi_d \\ \psi_q \\ \psi_0 \end{bmatrix} \tag{6}$$

The flux linkages in *dq0*-axis are given by:

$$\begin{bmatrix} \psi_d \\ \psi_q \\ \psi_0 \end{bmatrix} = L_{dq0}\begin{bmatrix} i_d \\ i_q \\ i_0 \end{bmatrix} \tag{7}$$

and the L_{dq0} are calculated by $P^{-1}L_sP$, and given by:

$$L_{dq0} = \begin{bmatrix} L_d & L_{qd} & L_{0d} \\ L_{dq} & L_q & L_{0q} \\ L_{d0} & L_{q0} & L_0 \end{bmatrix} \tag{8}$$

The same method for calculating L_{dq0} as detailed in [18] has been adopted in this paper. It is worth noting that the *dq0*-axis self-inductances, i.e. L_d, L_q and L_0, contain non-zero dc components and superimpose with the spatial harmonic components with order $6k$, k = 1, 2, 3… However, the *dq0*-axis mutual-inductances do not have the dc component and only contain harmonic components. For example, the harmonic orders are $6k$, with k = 1, 2, 3… for L_{qd}, and $3k$ with k = 1, 3, 5… for L_{d0} and L_{q0}. Fig. 2 shows the waveform of *dq0*-axis self- and mutual-inductances. To simplify the analyses, the magnitude of the nth order inductance harmonic will be written as $L_{xx,n}$ in the following sections. For example, $L_{d,dc}$ represents the dc component of L_d, $L_{d,6}$ represents the magnitude of the 6th order L_d harmonic, etc.

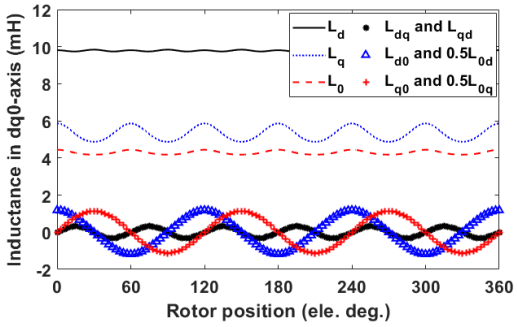

Fig. 2. *dq0*-axis inductances *vs* rotor position.

The instantaneous power in the *dq0*-axis frame can be calculated as:

$$\begin{aligned} P_{in} &= [v_a \quad v_b \quad v_c]\begin{bmatrix} i_a \\ i_b \\ i_c \end{bmatrix} = \left(P^{-1}\begin{bmatrix} v_d \\ v_q \\ v_0 \end{bmatrix}\right)^{-1} P\begin{bmatrix} i_d \\ i_q \\ i_0 \end{bmatrix} \\ &= \frac{3}{2}\left(v_d i_d + v_q i_q + 2v_0 i_0\right) \end{aligned} \tag{9}$$

Therefore, the instantaneous torque T_e can be determined from the instantaneous power as:

$$\omega_m T_e = P_{in} - P_{cop} - \frac{dW_m}{dt} \quad (10)$$

where ω_m is the mechanical speed, P_{cop} represents the resistive loss. W_m is the stored energy in the machine, which can be calculated by flux-current map, and for the linear case, the stored magnetic energy can be calculated by [19]

$$W_m = \frac{1}{2}\sum_{i=a,b,c} \psi_i i_i = \frac{3}{2}\times\frac{1}{2}(\psi_d i_d + \psi_q i_q + 2\psi_0 i_0) \quad (11)$$

Substituting (6), (9) and (11) into (10), yields:

$$T_e = \frac{3}{2}p\left(\psi_d i_q - \psi_q i_d + \frac{1}{2}i_d\frac{d\psi_d}{d\theta_e} + \frac{1}{2}i_q\frac{d\psi_q}{d\theta_e} + i_0\frac{d\psi_0}{d\theta_e} - \frac{1}{2}\psi_d\frac{di_d}{d\theta_e} - \frac{1}{2}\psi_q\frac{di_q}{d\theta_e} - \psi_0\frac{di_0}{d\theta_e}\right) \quad (12)$$

Without considering the current harmonics in the *abc*-axis, the *dq0*-axis currents will be constant as can be calculated by (13), and only the first four terms on the right hand side of (12) will produce average torque and torque ripple.

$$\begin{bmatrix} i_d \\ i_q \\ i_0 \end{bmatrix} = \begin{bmatrix} I_{d,dc} \\ I_{q,dc} \\ 0 \end{bmatrix} \quad (13)$$

Therefore, the instantaneous torque due to fundamental current can be obtained:

$$T_f = T_{f,dc} + T_{f,rip} \quad (14)$$

In (14), the average torque $T_{f,dc}$ and torque ripple $T_{f,rip}$ can be calculated as:

$$T_{f,dc} = \frac{3}{2}p(L_{d,dc} - L_{q,dc})I_{d,dc}I_{q,dc} \quad (15)$$

and

$$T_{f,rip} = \frac{3}{2}p\left\{\sum_{n=6,12,18,\dots}(L_{d,n} - L_{q,n} + nL_{dq,n})I_{d,dc}I_{q,dc}\cos(n\theta_e) - \sum_{n=6,12,18,\dots}\frac{n}{2}(L_{d,n}I_{d,dc}^2 + L_{q,n}I_{q,dc}^2)\sin(n\theta_e) + \sum_{n=6,12,18,\dots}L_{dq,n}(I_{q,dc}^2 - I_{d,dc}^2)\sin(n\theta_e)\right\} \quad (16)$$

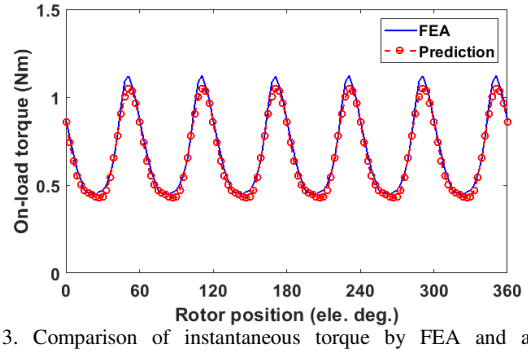

Fig. 3. Comparison of instantaneous torque by FEA and analytical predictions with 5Arms fundamental current.

It can be found that the average torque is only produced by the dc components of the *dq*-axis inductances. Moreover, the frequency of torque ripple is a multiple of the 6th order for the 3-phase MCSRMs. And the nth order torque ripple is due to the interaction between the nth order *dq0*-axis inductance and the fundamental current (dc component in *dq*-axis). For accurate prediction and easy implementation, the 6th and 12th order inductance harmonics will be considered in this paper, as shown in Fig. 3.

III. Instantaneous Torque Equation With Current Harmonics Injected

When the harmonic current is injected, by way of example, the expression of phase a current can be written as:

$$I_a = I_f\sin(\theta_e + \beta_f) + I_v\sin(v\theta_e + \beta_v) \quad (17)$$

where I_f and β_f are the magnitude and phase angle of the fundamental current, respectively. I_v and β_v are the magnitude and phase angle for the v^{th} order harmonic current. It is worth noting that the torque model with current harmonic injection will be investigated for two separate cases, i.e. zero-sequence current harmonics in *dq0*-axis frame (3rd order current harmonic in *abc*-axis frame) and non-zero-sequence current harmonics in *dq0*-axis frame (5th and 7th current harmonics in *abc*-axis frame), as detailed in Appendix.

A. Torque due to Zero-Sequence Current

The 3rd order current harmonic injection will bring extra zero-sequence current component for a balanced 3-phase system. This section will investigate the torque contribution due to the zero-sequence current. And the *dq0*-axis current equation is given by:

$$\begin{bmatrix} i_d \\ i_q \\ i_0 \end{bmatrix} = \begin{bmatrix} I_{d,dc} \\ I_{q,dc} \\ I_{0,3}\cos(3\theta_e + \varphi_0) \end{bmatrix} \quad (18)$$

In this case, the coupling effect between the zero-sequence and *dq*-axis current cannot be neglected. The flux linkage due to coupling effect can be written as (19).

$$\begin{bmatrix} \psi_d \\ \psi_q \\ \psi_0 \end{bmatrix}\Bigg|_{i_0} = \begin{bmatrix} 0 & 0 & L_{0d} \\ 0 & 0 & L_{0q} \\ L_{d0} & L_{q0} & L_0 \end{bmatrix}\begin{bmatrix} i_d \\ i_q \\ i_0 \end{bmatrix} \quad (19)$$

Putting (18) and (19) into (12), the torque due to zero-sequence current T_{zero} can be calculated by:

$$T_{zero} = \frac{3}{2}p\left\{\sum_{n=3,9,15,\dots}(L_{d0,n} - nL_{q0,n})I_{q,dc}I_{0,3}\cos((n-3)\theta_e - \varphi_0) + \sum_{n=3,9,15,\dots}(L_{q0,n} - nL_{d0,n})I_{d,dc}I_{0,3}\sin((n-3)\theta_e - \varphi_0) + \sum_{n=3,9,15,\dots}(L_{d0,n} - nL_{q0,n})I_{q,dc}I_{0,3}\cos((n+3)\theta_e + \varphi_0) + \sum_{n=3,9,15,\dots}(L_{q0,n} - nL_{d0,n})I_{d,dc}I_{0,3}\sin((n+3)\theta_e + \varphi_0) - \sum_{n=6,12,18,\dots}\frac{n}{4}L_{0,n}{I_{0,3}}^2(\sin((n+6)\theta_e + 2\varphi_0) + \sin((n-6)\theta_e - 2\varphi_0) + 2\sin(n\theta_e))\right\} \quad (20)$$

It is obvious that once the zero-sequence current is not equal to zero, there will be a multiple of the 6th order torque harmonics in the resultant torque for a 3-phase MCSRM. Moreover, when the coefficient of θ_e in (20) is equal to 0, i.e. n = 3 for the first two terms and n = 6 for the last term, an extra average torque can be obtained. Therefore, the first two terms and the last term will contribute to average torque when the 3rd order current harmonic is injected, as shown below:

$$T_{zero,dc} = \frac{3}{2}p\left(L_{d0,3} - 3L_{q0,3}\right)I_{q,dc}I_{0,3}\cos(-\varphi_0) + \frac{3}{2}p\left(L_{q0,3} - 3L_{d0,3}\right)I_{d,dc}I_{0,3}\sin(-\varphi_0) - \frac{3}{8}pnL_{0,6}{I_{0,3}}^2\sin(-2\varphi_0) \quad (21)$$

Since the last term on the right hand side of (21) is much smaller than the other two terms, it can be neglected and the average torque can be rewritten as:

$$T_{zero,dc} = T\sin(\varphi_0 + \varphi) \quad (22)$$

where

$$T = \sqrt{A^2 + B^2} \quad (23)$$

$$\tan\varphi = \frac{B}{A} \quad (24)$$

with

$$\begin{cases} A = -\frac{3}{2}p\left(L_{q0,3} - 3L_{d0,3}\right)I_{d,dc}I_v \\ B = \frac{3}{2}p\left(L_{d0,3} - 3L_{q0,3}\right)I_{q,dc}I_v \end{cases} \quad (25)$$

B. *Torque due to Non-Zero-Sequence Current*

This section will investigate the torque model due to a non-zero-sequence current. In order to inject the 5th or 7th order current harmonic in the *abc*-axis frame, the 6th order current harmonic has to be injected in the *dq*-axis, as described by (26). The difference between injecting the 5th and 7th order current harmonics has been shown in TABLE II (See details in Appendix).

$$\begin{bmatrix} i_d \\ i_q \\ i_0 \end{bmatrix} = \begin{bmatrix} I_{d,dc} + I_{d,6}\cos(6\theta_e + \varphi_d) \\ I_{q,dc} + I_{q,6}\sin(6\theta_e + \varphi_q) \\ 0 \end{bmatrix} \quad (26)$$

Putting (7), (8) and (26) in (12), gives:

$$\begin{aligned} T_{non-zero} = \frac{3}{2}p\Big\{&\frac{1}{2}\left(L_{d,dc} - L_{q,dc}\right)I_{d,6}I_{q,6}\left(\sin(12\theta_e + \varphi_d + \varphi_q) - \sin(\varphi_d - \varphi_q)\right) \\ &+\left(L_{d,dc} - L_{q,dc}\right)\left(I_{q,dc}I_{d,6}\cos(6\theta_e + \varphi_d) + I_{d,dc}I_{q,6}\sin(6\theta_e + \varphi_q)\right) \\ &\sum_{n=6,12,18,\dots}\frac{1}{2}\left(L_{d,n} - L_{q,n}\right)I_{d,n}I_{q,dc}\left(\cos\left((n+6)\theta_e + \varphi_d\right) + \cos\left((n-6)\theta_e - \varphi_d\right)\right) \\ &+\sum_{n=6,12,18,\dots}\frac{1}{2}\left(L_{d,n} - L_{q,n}\right)I_{d,dc}I_{q,n}\left(\sin\left((n+6)\theta_e + \varphi_q\right) - \sin\left((n-6)\theta_e - \varphi_q\right)\right) \\ &-\sum_{n=6,12,18,\dots}L_{dq,n}I_{q,dc}I_{q,n}\left(\cos\left((n+6)\theta_e + \varphi_q\right) - \cos\left((n-6)\theta_e - \varphi_q\right)\right) \\ &-\sum_{n=6,12,18,\dots}L_{dq,n}I_{d,dc}I_{d,n}\left(\sin\left((n+6)\theta_e + \varphi_d\right) + \sin\left((n-6)\theta_e - \varphi_d\right)\right) \\ &-\sum_{n=6,12,18,\dots}\frac{n}{2}L_{d,n}I_{d,dc}I_{d,n}\left(\sin\left((n+6)\theta_e + \varphi_d\right) + \sin\left((n-6)\theta_e - \varphi_d\right)\right) \\ &+\sum_{n=6,12,18,\dots}\frac{n}{2}L_{q,n}I_{q,dc}I_{q,n}\left(\cos\left((n+6)\theta_e + \varphi_q\right) - \cos\left((n-6)\theta_e - \varphi_q\right)\right) \\ &+\sum_{n=6,12,18,\dots}\frac{n}{2}L_{dq,n}I_{d,dc}I_{q,n}\left(\sin\left((n+6)\theta_e + \varphi_q\right) - \sin\left((n-6)\theta_e - \varphi_q\right)\right) \\ &+\sum_{n=6,12,18,\dots}\frac{n}{2}L_{dq,n}I_{q,dc}I_{d,n}\left(\cos\left((n+6)\theta_e + \varphi_d\right) + \cos\left((n-6)\theta_e - \varphi_d\right)\right)\Big\} \end{aligned} \quad (27)$$

It has been found that if the 6th order current harmonic is injected in the *dq*-axis, there will be a multiple of the 6th order torque harmonics in the resultant instantaneous torque. Moreover, it is also found that the average torque can be obtained when *n* is 6. Therefore, the average torque due to the 6th order current harmonic can be calculated by:

$$T_{non-zero,dc} = T\sin(\varphi_d + \varphi) \quad (28)$$

where

$$T = \begin{cases} \sqrt{(A-D)^2 + (B-C)^2} & for\ \varphi_d = \varphi_q + \pi\ (5^{th}\ injection) \\ \sqrt{(A+D)^2 + (B+C)^2} & for\ \varphi_d = \varphi_q \quad (7^{th}\ injection) \end{cases} \quad (29)$$

and

$$\tan\varphi = \begin{cases} \frac{A-D}{B-D} & for\ \varphi_d = \varphi_q + \pi\ (5^{th}\ injection) \\ \frac{A+D}{B+D} & for\ \varphi_d = \varphi_q \quad (7^{th}\ injection) \end{cases} \quad (30)$$

with

$$\begin{cases} A = \left(\frac{\left(L_{d,6} - L_{q,6}\right)}{2} + 3L_{dq,6}\right)I_{q,dc}I_v \\ B = \left(3L_{d,6} + L_{dq,6}\right)I_{d,dc}I_v \\ C = \left(\frac{\left(L_{d,6} - L_{q,6}\right)}{2} + 3L_{dq,6}\right)I_{d,dc}I_v \\ D = \left(-3L_{q,6} + L_{dq,6}\right)I_{q,dc}I_v \end{cases} \quad (31)$$

It is worth noting that based on the proposed *dq0*-axis model, the current harmonic (magnitude and phase angle) can also be selected to reduce the torque ripple by using the same method in [12], and the results are shown in Fig. 4. Generally, a good agreement has been observed at a phase rms current of 5A. It is worth noting that similarly as the model in *abc*-axis frame, the proposed model in *dq0*-axis cannot predict the torque ripple accurately when machine is highly saturated, due to the fact that (11) cannot calculate the magnetic store energy for non-linear condition. This would be the main drawback of the proposed analytical torque modelling.

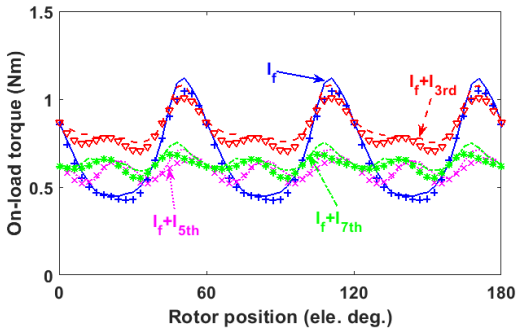

Fig. 4. Comparison of instantaneous torque by FEA and analytical predictions with/without current harmonic injection. Phase current is 5Arms. (Line: FEA; Mark: Analytical prediction).

IV. Dynamic Performance With Current Harmonic Injection

Although the harmonic current injection can reduce torque ripple and the 3rd order harmonic current can even increase the average torque, the interaction between the inductance and current harmonics will lead to non-negligible distortion in the phase voltage, which could deteriorate the

dynamic performances of the MCSRM. The proposed *dq0*-axis model not only provides a powerful insight into the mechanism of torque generation, but also simplifies the investigation of dynamic performance, such as torque-speed curves, efficiency maps, etc. Therefore, based on proposed model, the influences of different current harmonic injections on the dynamic performance for the MCSRM are carried out in this paper.

A. *Torque-Speed Curve for Fundamental Current Supply*

For the MCSRM supplied by a voltage source inverter with space vector pulse-width-modulation (SVPWM) control, its phase current and voltage should satisfy the following conditions for a full range of speed:

$$\sqrt{{v_d}^2 + {v_q}^2} \le V_{max} = \frac{V_{dc}}{\sqrt{3}} \quad (32)$$

$$\sqrt{{i_a}^2 + {i_q}^2} \le I_{max} \quad (33)$$

where V_{max} and I_{max} are the voltage and current constraints of the inverter. Fig. 5 shows the dynamic voltage variation considering both the dc and harmonic component in the *dq0*-axis flux linkage. A good agreement has been observed between for 2D-FEA and analytical prediction. As expected, once the flux-linkage harmonics $\psi_{dq0,h}$ due to inductance and/or current harmonics are considered, there is significant distortion in the phase voltage. This means that with increasing rotor speed, the peak voltage will reach the inverter's voltage limit earlier than that without considering the flux linkage harmonics. As a result, the flux weakening capability can be reduced. Fig. 6 shows the torque-speed curves when the current constraint of the inverter is 7.07 A (5 Arms), and the dc link voltage is 24V. It is found that the torque is significantly reduced during flux weakening operation and the base speed shows 25% reduction once the voltage distortion due to inductance harmonics is considered.

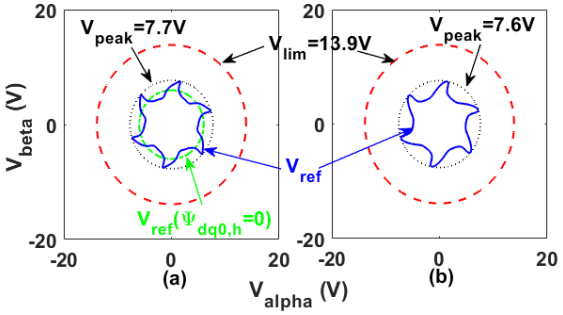

Fig. 5. $\alpha\beta$-axis voltages for fundamental current. ($I_{max} = 7.07A$, $\omega = 200rpm$ and $V_{dc} = 24V$). (a) 2D-FEA and (b) Analytical prediction.

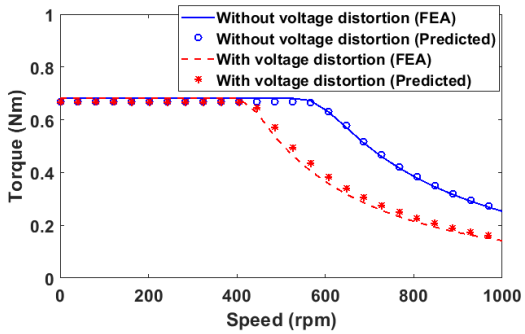

Fig. 6. Torque-speed curves for fundamental current. *I*=5Arms and V_{dc}=24V.

B. *Torque-Speed Curve with Current Harmonic Injection*

As example, Fig. 7 shows the current waveform of the 3rd order current harmonic injection. As can be seen that for the same rms current, the peak current is larger than that of the fundamental current. This means that the selected 3rd order current harmonic reaches the current limit earlier than the pure sinewave current supply. Therefore, the rms current should be reduced to keep the peak current at the same level after injecting the current harmonic. It will happen for the 5th and 7th order current harmonic injections as well. For completeness, the dynamic performance will be investigated in two cases, i.e. one is constant rms current condition (CRMS), while the other is constant peak current condition (CPC).

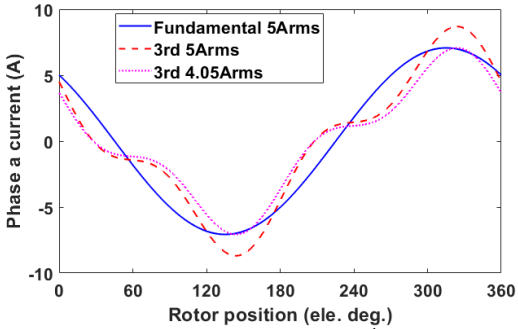

Fig. 7. Phase a current waveform with the 3rd order current harmonic injection.

The same as fundamental current supply in Fig. 5, the voltage vector with 5th and 7th current harmonic injection has also been shown in Fig. 8, and only the analytically predicted results have been presented. It is obvious that the distortion in the voltage is significant, especially when current harmonics are injected. And compared with pure sinewave current supply in Fig. 5, the 5th and 7th current harmonic injection will lead to the machine reach the inverter's voltage limit even faster.

It is worth noting that, different from the 5th and 7th harmonic current injections, the 3rd order current harmonic injection will bring extra zero-sequence current. Therefore, it requires a special control strategy to control the injected zero-sequence current. This can be achieved using the 3-dimentional (3D) SVPWM [20]-[21], in which the neutral point of a 3-phase machine is connected to an extra half bridge leg. It has been found that without considering the over modulation, the voltage limit of the 3D-SVPWM can be calculated by $\frac{V_{dc}}{\sqrt{3}}$, as shown in (34). Similar to the fundamental current supply in section IV.A, the voltage distribution with the 3rd order current harmonic injection can be limited in a sphere with a radius of $\frac{V_{dc}}{\sqrt{3}}$, as shown in Fig. 9.

$$\sqrt{{v_d}^2 + {v_q}^2 + {v_0}^2} \le V_{max} = \frac{V_{dc}}{\sqrt{3}} \quad (34)$$

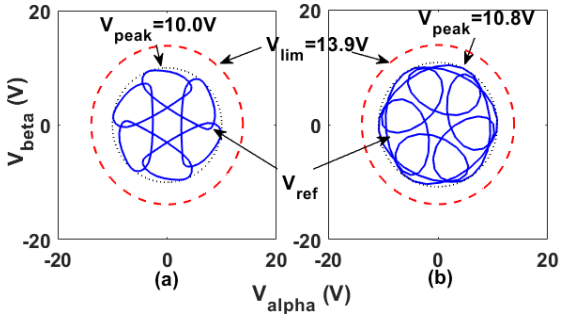

Fig. 8. $\alpha\beta$-axis voltages with voltage distortion. (a) I_f+I_{5th} and (b) I_f+I_{7th}. ($I_{rms} = 5Arms$, $\omega = 200rpm$ and $V_{dc} = 24V$).

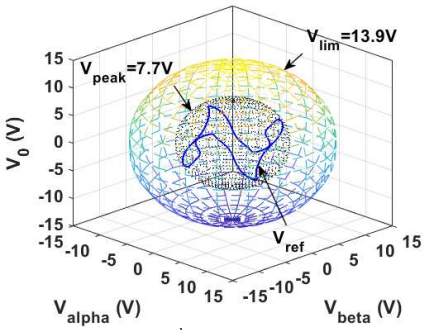

Fig. 9. $\alpha\beta 0$-axis voltages with the 3rd order current injection and with voltage distortion. ($I_{rms} = 5Arms$, $\omega = 200rpm$ and $V_{dc} = 24V$).

Therefore, the torque-speed curve under CRMS condition has been calculated, as shown in Fig. 10. A good agreement can be observed between the FEA and analytical predictions. It is also found that the base speed of the MCSRM could be reduced after injecting the current harmonics, especially for the 5th and 7th order current harmonics. It is mainly due to the fact that these current harmonics cause significant voltage distortion which limits the flux weakening capability. However, the 3rd order current harmonic can increase the average torque in constant torque region and maintain similar torque level as fundamental current supply in flux weakening region.

Fig. 11 shows the torque-speed curves under constant peak current condition. Using the 3rd order current harmonic injection as example, due to the fact that the rms current is reduced by 19% (see Fig. 7), the average torque can be reduced to $(1-0.19)^2 \times 100 = 65.6\%$ of that of the CRMS condition. However, it is worth noting that the dynamic performance for the two cases (CRMS or CPC condition) are the same in flux weakening region. This is due to the fact that in the flux weakening region, machine is limited by the voltage rather than the current, meaning that with the same machine parameters, the torque-speed performance of the two cases should be the same. This is also the case for other order current harmonic injections.

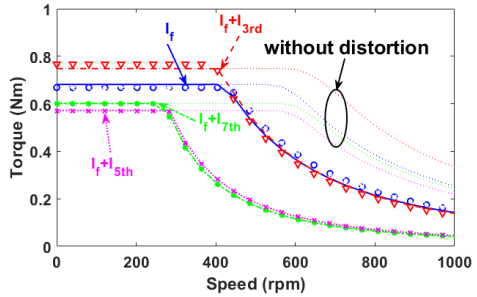

Fig. 10. Torque-speed curves after current harmonic injection with considering the voltage distortion under CRMS condition. I_{rms}=5Arms and V_{dc}=24V. (Line: FEA; Mark: Analytical prediction).

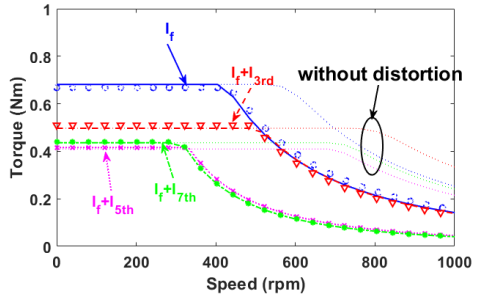

Fig. 11. Torque-speed curves after current harmonic injection with considering the voltage distortion under CPC condition. I_{peak}=7.07A and V_{dc}=24V. (Line: FEA; Mark: Analytical prediction).

V. Experimental Validation

In order to validate the predictions using the proposed current harmonic injection method, a single layer 12s/8p MCSRM built in [22] has been adopted for experimental tests. The machine specifications are shown in TABLE I. Fig. 12 shows the test rig setup for validating the proposed harmonic current injection method. The experiments with the proposed methods under dynamic conditions are described in the following sections.

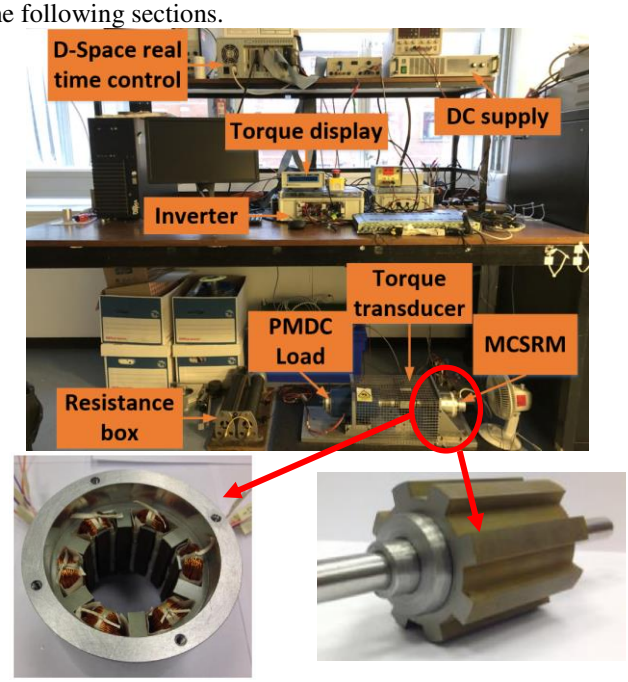

Fig. 12. Test rig and prototype machine for dynamic tests.

Two types of dynamic tests including transient current, speed and torque as well as torque-speed and efficiency-speed curves are also carried out. The implementing method for the 3rd order current harmonic injection is detailed in [12]. A 3 phase 4-leg inverter was adopted for injecting the 3rd order current harmonic.

The first test evaluated the performance of the proposed current injection method at transient state. Therefore, the machine is operating under speed control, and a permanent magnet dc generator is utilized as the load. At the beginning, the test machine rotates at 50rpm and after 3s, the speed demand increases to 200rpm. The harmonic current can be added into the *dq0*-axis reference current directly. The phase a currents are shown in Fig. 13 (a) and the speed and torque of the MCSRM with and without the current harmonic injection are shown in Fig. 13 (b) and (c), respectively. It can be seen that the speed and torque ripple suppression by the proposed method is not compromised at transient-state. Moreover, the transient time from 50rpm to 200rpm can even be reduced by more than 10% after injecting the 3rd order current harmonic, which is due to the extra torque produced by such harmonic current injection.

Fig. 14 shows the torque spectra at different speeds. A clear reduction in the 6th order torque ripple can be observed at both low and relatively higher speeds. However, it is also observed that there are some low frequency harmonics in the on-load torque. This is mainly due to the manufacturing tolerance of the prototype machine, the unavoidable imbalance in the test rig and also the torque ripple introduced by the load generator.

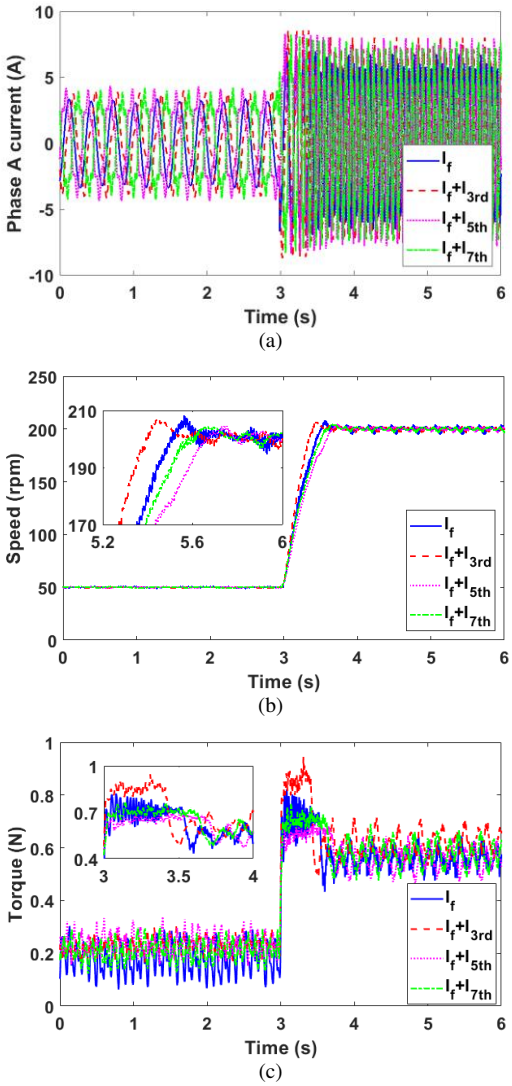

Fig. 13. Transient state results with/without current harmonic injection. $I_{rms} = 5Arms$ and V_{dc}=24V (a) Phase a currents, (b) speeds and (c) on-load torques.

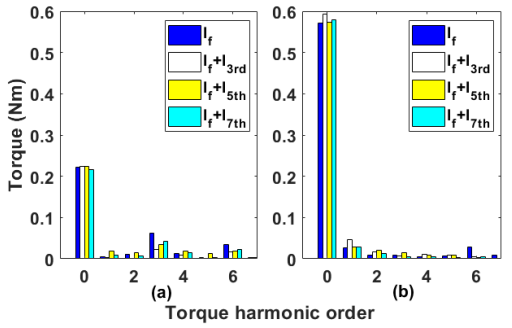

Fig. 14. Torque spectra at different speeds. (a) $\omega = 50rpm$ and (b) $\omega = 200rpm$.

The second test investigated the dynamic performance by implementing the current harmonic injection method. It is worth mentioning that in order to ease the winding process of the prototype machine, smaller copper wires have been deliberately used in the prototype machine, leading to higher phase resistance. As a result, if V_{dc} is still kept at 24V as in Section IV, there will be no constant torque region. Therefore, a higher V_{dc} of 40V has been used in this test. Fig. 15 shows the torque-speed and efficiency-speed curves for the test machine. Overall, the measured torque-speed and efficiency-speed curve match well with the predictions. As expected, with the 3rd order current harmonic injection, the machine produces more than 10% extra torque at the constant torque region, and slightly higher torque during the flux-weakening operation. In addition, the 3rd order current harmonic injection can also improve the machine efficiency for the investigated speed range, while the 5th and 7th order current harmonic injections can only reduce the machine efficiency in full speed range. It is worth noting that the lower efficiency is mainly due to relatively higher phase resistance, which leads to higher copper loss.

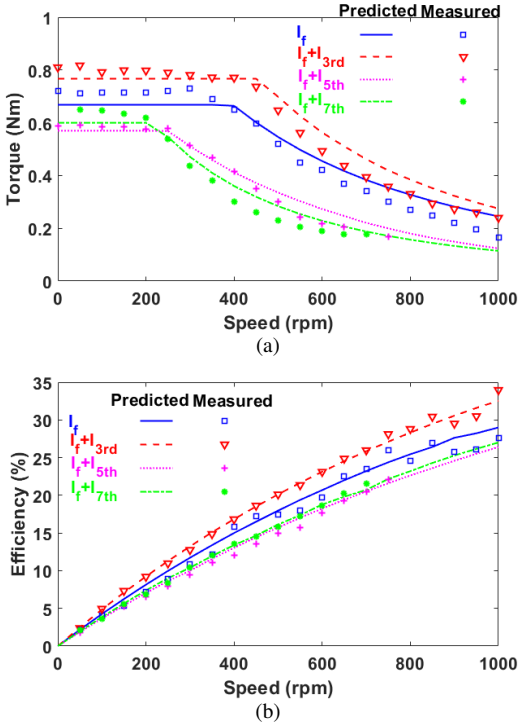

Fig. 15. Predicted and measured torque-speed and efficiency-speed curves. ($I_{rms} = 5Arms$ and V_{dc}=40V) (a) torque-speed curve and (b) efficiency-speed curve.

VI. Conclusion

This paper proposes an analytical torque model based on the *dq0*-axis frame for doubly salient synchronous reluctance machines with current harmonic injection. Such analytical torque model is essential for simplifying the investigation of dynamic performance such as torque-speed curve and efficiency maps. In addition, details have been provided for showing how to inject harmonic currents in *dq0*-axis frame for 3rd, 5th and 7th order current harmonic injections.

Due to the interaction between current and inductance harmonics, there will be significant voltage distortion, which will in turn affect machine dynamic performance (flux weakening capability) such as torque-speed curves. The results have shown that, in the constant torque region (or constant torque region), different from the 5th and 7th order harmonic current injections, the 3rd order current harmonic can increase the average torque. In flux weakening region (or constant power region), the 3rd order harmonic current injection can achieve similar torque level as the fundamental current supply while the 5th and 7th order harmonic currents generally reduce the output torque. The proposed analytical modelling and current harmonic injection are both validated by FE simulations and dynamic tests.

APPENDIX

In order to inject the current harmonics as proposed in [12] into *dq0*-axis, the transformation of *dq0*-axis currents to *abc*-axis currents has been analysed in this section. It is worth noting that the understanding of the transformation effect of current harmonics in *dq0*-axis frame to *abc*-axis frame and vice versa is essential for investigating the dynamic performance and also for the experimental validation. The general current equation in *dq0*-axis is given by

$$\begin{cases} i_d = I_{d,0} + I_{d,k}\cos(k\theta_e + \alpha_{d,k}) \\ i_q = I_{q,0} + I_{q,k}\sin(k\theta_e + \alpha_{q,k}) \\ i_0 = i_{0,k}\sin(k\theta_e + \alpha_{0,k}) \end{cases} \tag{35}$$

where $I_{d,0}$ and $I_{q,0}$ are the dc component in *dq*-axis, respectively. k, $I_{dq0,k}$ and $\alpha_{dq0,k}$ represent the order (k=3, 6, 9…), magnitude and phase angle of the k^{th} harmonic, respectively. After employing the inverse Park transformation, the currents in *abc*-axis reference frame can be simplified as

$$\begin{aligned} i_a(\theta_e) &= i_1^*(\theta_e) + i_{k-1}^*(\theta_e) + i_{k+1}^*(\theta_e) + i_0 \\ i_b(\theta_e - 120°) &= i_1^*(\theta_e - 120°) + i_{k-1}^*(\theta_e - 120°) \\ &\quad + i_{k+1}^*(\theta_e - 120°) + i_0 \\ i_c(\theta_e + 120°) &= i_1^*(\theta_e + 120°) + i_{k-1}^*(\theta_e + 120°) \\ &\quad + i_{k+1}^*(\theta_e + 120°) + i_0 \end{aligned} \tag{36}$$

with

$$\begin{cases} i_1^*(\theta_e) = i_1\sin(\theta_e + \alpha_1) \\ i_{k-1}^*(\theta_e) = i_{k-1}\sin[(k-1)\theta_e + \alpha_{k-1}] \\ i_{k+1}^*(\theta_e) = i_{k+1}\sin[(k+1)\theta_e + \alpha_{k+1}] \end{cases} \tag{37}$$

The magnitude and phase angle in (37) can be calculated by

$$\begin{cases} i_m = \sqrt[2]{b^2 + a^2} \\ \tan\alpha_m = \dfrac{b}{a} \end{cases} \quad m = 1, k-1 \text{ and } k+1$$

$$a = \begin{cases} -I_{q,0} & m = 1 \\ 0.5(-I_{d,k}\sin\alpha_{d,k} + I_{q,k}\sin\alpha_{q,k}) & m = k-1 \\ 0.5(-I_{d,k}\sin\alpha_{d,k} - I_{q,k}\sin\alpha_{q,k}) & m = k+1 \end{cases} \tag{38}$$

$$b = \begin{cases} I_{d,0} & m = 1 \\ 0.5(I_{d,k}\cos\alpha_{d,k} - I_{q,k}\cos\alpha_{q,k}) & m = k-1 \\ 0.5(I_{d,k}\cos\alpha_{d,k} + I_{q,k}\cos\alpha_{q,k}) & m = k+1 \end{cases}$$

Based on (35) and (36), it can be found that the magnitude and phase angle of *0*-axis current before and after Park Transformation will not change. Therefore, the 3rd order current harmonic can be simply injected by supplying exactly the same 3rd order current harmonic into *0*-axis.

Moreover, it can also be found that in order to inject the 5th and 7th order current harmonics, both the 6th order current harmonic in *dq*-axis have to be injected. To clarify the difference between the 5th and 7th current harmonic injections, further analysis for (36)-(38) has been done. Some assumptions have been made to simplify the method, i.e. the magnitude of injected current harmonics in both *d*- and *q*-axes are the same.

$$I_{d,k} = I_{q,k} \tag{39}$$

To cancel the (k+1)th order current harmonic in (36), i_{k+1} in (37) should be equal to 0. Hence, components in (38) with m=k+1 must be "0" at the same time, as shown in (40).

$$\begin{cases} a = 0.5(-I_{d,k}\sin\alpha_{d,k} - I_{q,k}\sin\alpha_{q,k}) = 0 \\ b = 0.5(I_{d,k}\cos\alpha_{d,k} + I_{q,k}\cos\alpha_{q,k}) = 0 \end{cases} \tag{40}$$

And it can be solved as

$$\alpha_{d,k} = \alpha_{q,k} + \pi \tag{41}$$

By substituting (39) and (41) into (38), the (k-1)th order current harmonic can be easily calculated by

$$\begin{cases} i_{k-1}^*(\theta_e) = I_{d,k}\sin[(k-1)\theta_e + \alpha_{d,k}] \\ i_{k+1}^*(\theta_e) = 0 \end{cases} \tag{42}$$

The same method has been utilized to cancel the (k-1)th harmonic. When the injected *dq*-axis harmonics satisfy the condition as

$$\alpha_{d,k} = \alpha_{q,k} \tag{43}$$

then the (k+1)th order current harmonic can be obtained as

$$\begin{cases} i_{k-1}^*(\theta_e) = 0 \\ i_{k+1}^*(\theta_e) = I_{d,k}\sin[(k+1)\theta_e + \alpha_{d,k}] \end{cases} \tag{44}$$

After comparing (42) and (44) with current harmonic equation (17) in *abc*-axis. The implementation of current harmonic injections in *dq0*-axis frame can be concluded in TABLE II. When the magnitudes of *dq*-axis currents are the same ($I_{d,k} = I_{q,k} = I_v$), and if $\alpha_{d,k} = \alpha_{q,k} + \pi = \beta_v$, there is only ($k$-1)th order current harmonic in the 3-phase currents. But if $\alpha_{d,k} = \alpha_{q,k} = \beta_v$, there is only ($k$+1)th order current harmonic in the 3-phase currents.

TABLE II IMPLEMENTATION OF CURRENT HARMONIC INJECTIONS IN DQ-AXIS FRAME

v \ $I_{dq0,k}$	$I_{d,k}$	$\alpha_{d,k}$	$I_{q,k}$	$\alpha_{q,k}$	$I_{0,k}$	$\alpha_{0,k}$
k	0	-	0	-	i_v	β_v
$k-1$	i_v	β_v	i_v	$\beta_v+\pi$	0	-
$k+1$	i_v	β_v	i_v	β_v	0	-

Note: k=3, 6, 9… *abc*-axis frame harmonic orders are k, $k-1$ or $k+1$, while in *dq0*-axis frame, they are either 0 or k.

REFERENCES

[1] T. J. E. Miller, "Optimal design of switched reluctance motors," *IEEE Trans. Ind. Electron.,* vol. 49, no. 1, pp. 15-27, Feb. 2002.

[2] W. Hua, H. hua, N. Dai, G. Zhao, and M. Cheng, "Comparative study of switched reluctance machines with half-and full-teeth-wound windings," *IEEE Trans. Ind. Electron.,* vol. 63, no. 3, pp. 1414-1424, March 2016.

[3] J. Li and Y. Cho, "Investigation into reduction of vibration and acoustic noise in switched reluctance motors in radial force excitation and frame transfer function aspects," *IEEE Trans. Magn.,* vol. 45, no. 10, pp. 4664-4667, Oct. 2009.

[4] D. E. Cameron, J. H. Lang, and S. D. Umans, "The origin and reduction of acoustic noise in doubly salient variable-reluctance motors," *IEEE Trans. Ind. Appl.,* vol. 28, no. 6, pp. 1250-1255, Nov.-Dec. 1992.

[5] F. Daldaban and N. Ustkoyuncu, "Multi-layer switched reluctance motor to reduce torque ripple," *Energy Conversion and Management,* vol. 49, no. 5, pp. 974-979, May 2008.

[6] H. Y. Yang, Y. C. Lim, and H. C. Kim, "Acoustic noise/vibration reduction of a single-phase SRM using skewed stator and rotor," *IEEE Trans. Ind. Electron.,* vol. 60, no. 10, pp. 4292-4300, Oct. 2013.

[7] S. K. Sahoo, S. Dasgupta, S. K. Panda, and J. X. Xu, "A lyapunov function-based robust direct torque controller for a switched reluctance motor drive system," *IEEE Trans. Power Electron.,* vol. 27, no. 2, pp. 555-564, Feb. 2012.

[8] H. J. Brauer, M. D. Hennen, and R. W. D. Doncker, "Control for polyphase switched reluctance machines to minimize torque ripple and decrease ohmic machine losses," *IEEE Trans. Power Electron.,* vol. 27, no. 1, pp. 370-378, 2012.

[9] X. Liu, Z. Q. Zhu, M. Hasegawa, A. Pride, and R. Deodhar, "Investigation of PWMs on vibration and noise in SRM with sinusoidal bipolar excitation," presented at the in Proc. 21th IEEE International Symposium on Ind. Electron., Hangzhou, China, pp. 674-679, 2012.

[10] G. Feng, C. Lai, and N. C. Kar, "An analytical solution to optimal stator current design for PMSM torque ripple minimization with minimal machine losses," *IEEE Trans. Ind. Electron.,* vol. 64, no. 10, pp. 7655-7665, Oct. 2017.

[11] X. B. Liang, G. J. Li, J. Ojeda, M. Gabsi, and Z. X. Ren, "Comparative study of classical and mutually coupled switched reluctance motors using multiphysics finite-element modeling," *IEEE Trans. Ind. Electron.,* vol. 61, no. 9, pp. 5066-5074, Sep. 2014.

[12] G. Li, K. Zhang, Z. Q. Zhu, and G. Jewell, "Comparative studies of torque performance improvement for different doubly salient synchronous reluctance machines by current harmonic injection," *IEEE Trans. Energy Conver.,* pp. 1-1, Sep. 2018.

[13] K. Zhang, G. J. Li, Z. Q. Zhu, and G. W. Jewell, "Torque performance improvement of doubly salient synchronous reluctance machines by current harmonic injection," *in Proc. IEEE Int. Ele. Mach. & Dri Conf (IEMDC),* pp. 1222-1227, 12-15 May 2019.

[14] C. Jo, J. Seol, and I. Ha, "Flux-weakening control of ipm motors with significant effect of magnetic saturation and stator resistance," *IEEE Trans. Ind. Electron.,* vol. 55, no. 3, pp. 1330-1340, Mar. 2008.

[15] F. Niu, B. Wang, A. S. Babel, K. Li, and E. G. Strangas, "Comparative evaluation of direct torque control strategies for permanent magnet synchronous machines," *IEEE Trans. Power Electron.,* vol. 31, no. 2, pp. 1408-1424, 2016.

[16] E. Trancho, E. Ibarra, A. Arias, I. Kortabarria, J. Jurgens, L. Marengo, *et al.*, "Pm-assisted synchronous reluctance machine flux weakening control for EV and HEV applications," *IEEE Trans. Ind. Electron.,* vol. 65, no. 4, pp. 2986-2995, Apr. 2018.

[17] A. Chiba, F. Nakamura, T. Fukao, and M. A. Rahman, "Inductances of cageless reluctance-synchronous machines having nonsinusoidal space distributions," *IEEE Trans. Ind. Appl.,* vol. 27, no. 1, pp. 44-51, 1991.

[18] M. Farshadnia, M. A. M. Cheema, R. Dutta, J. E. Fletcher, and M. F. Rahman, "Detailed Analytical Modeling of Fractional-Slot Concentrated-Wound Interior Permanent Magnet Machines for Prediction of Torque Ripple," *IEEE Trans. Ind. Appl.,* vol. 53, no. 6, pp. 5272-5283, 2017.

[19] Z. Q. Zhu, B. Lee, L. Huang, and W. Chu, "Contribution of current harmonics to average torque and torque ripple in switched reluctance machines," *IEEE Trans. Magn.,* vol. 53, no. 3, pp. 1-1, Mar. 2017.

[20] R. G. Omar and R. H. Thejel, "Matlab/simulink modeling of four-leg voltage source inverter with fundamental inverter output voltages vector observation," *Iraq J. Electrical and Electronic Engineering,* vol. 10, no. 2, pp. 107-117, 2014.

[21] R. Zhang, V. H. Prasad, D. Boroyevich, and F. C. Lee, "Three-dimensional space vector modulation for four-leg voltage-source converters," *IEEE Trans. Power Electron.,* vol. 17, no. 3, pp. 314-326, May 2002.

[22] X. Y. Ma, G. J. Li, G. W. Jewell, Z. Q. Zhu, and H. L. Zhan, "Performance comparison of doubly salient reluctance machine topologies supplied by sinewave currents," *IEEE Trans. Ind. Electron.,* vol. 63, no. 7, pp. 4086 - 4096, Jul. 2016.